

**Cation-placement control in double-perovskite GdBaCo₂O₆ and its impact on magnetism via spin-state modification**

Journal:	<i>Journal of Materials Chemistry C</i>
Manuscript ID	TC-ART-04-2024-001498.R1
Article Type:	Paper
Date Submitted by the Author:	14-Jun-2024
Complete List of Authors:	Katayama, Tsukasa; Hokkaido University, research institute for electronic science Magara, Kento; The University of Tokyo Sakai, Shiro; RIKEN Zeng, Yijie; Hangzhou Dianzi University, School of Science Chikamatsu, Akira; Ochanomizu University, Department of Chemistry Hasegawa, Tetsuya; Tokyo Daigaku

Cation-placement control in double-perovskite $\text{GdBaCo}_2\text{O}_6$ and its impact on magnetism via spin-state modification

Tsukasa Katayama^{1,2*}, Kento Magara³, Shiro Sakai⁴, Yijie Zeng⁴, Akira Chikamatsu⁵, Tetsuya Hasegawa³

¹Research Institute for Electronic Science, Hokkaido University, Sapporo, Hokkaido, 001-0020, Japan

²JST-PRESTO, Kawaguchi, Saitama 332-0012, Japan

³Department of Chemistry, The University of Tokyo, Bunkyo-ku, Tokyo 113-0033, Japan

⁴Center for Emergent Matter Science, RIKEN, Wako, Saitama 351-0198, Japan

⁵Department of Chemistry, Faculty of Science, Ochanomizu University, 2-1-1 Otsuka, Bunkyo-ku, Tokyo 112-8610, Japan

E-mail: katayama@es.hokudai.ac.jp

Abstract

Double-perovskite $\text{GdBaCo}_2\text{O}_x$ exhibits remarkable magnetic properties, including half-metallicity, high magnetic anisotropy, and photoinduced magnetic phase transition. While manipulating these properties through cation arrangement is attractive, addressing the thermodynamic stability of the Gd/Ba order necessitates an unconventional synthesis approach. Herein, we report the synthesis of both A-site-ordered and -disordered $\text{GdBaCo}_2\text{O}_6$ films employing a combination of substrate-induced strain and low-temperature topochemical oxidation reactions. Both types of films displayed metallic and ferromagnetic behaviors. Interestingly, the A-site-disordered film exhibited superior magnetization ($11.5 \mu\text{B}/\text{f.u.}$ at 40 kOe), a higher Curie temperature ($T_C = 165 \text{ K}$), and lower resistivity compared to the A-site-ordered film ($9.5 \mu\text{B}/\text{f.u.}$ at 40 kOe; $T_C = 115 \text{ K}$). Theoretical calculations predicted that the alterations in the magnetic and conductive properties of the A-site-disordered film stem from a change in its Co spin states associated with a change in ion arrangement. This mechanism diverges from conventional double perovskites, where magnetic properties primarily stem from alterations in the combination of nearest-neighbor magnetic elements or lattice parameters without affecting the spin state. Our results highlight the potential of unconventional synthesis strategies in broadening the tunability of functionalities in double-perovskite materials and manipulating spin states through cation-placement control.

1. Introduction

Double perovskites, $AA'BB'O_6$, which feature two types of ordered A-site (A/A') or B-site (B/B') cations, exhibit fascinating properties that exceed those of single perovskites. These distinctive properties, including the ferrimagnetic half-metallicity of Sr_2FeMoO_6 and the extremely high magnetoresistivity of $NdBaMn_2O_6$, arise from complex lattice distortion and magnetic coupling between the ordered cations [1-3]. In particular, A-site-ordered double-perovskite cobaltites $GdBaCo_2O_x$ ($x = 5-6$) exhibit a rich variety of magnetic and electronic features, including high magnetoresistance [4,5], spin-crossover-associated metal-insulator transition [5], high magnetic anisotropy [5-7], half-metallicity [6], and magnetic field (H)- or photoinduced phase transitions from antiferromagnetic to ferromagnetic states [4,5,7-10]. Furthermore, $GdBaCo_2O_x$ exhibits excellent electrochemical properties, including fast oxygen-ion conductivity, anisotropic oxide-ion and proton conductivity, and efficient catalytic behavior [11-16].

The Gd/Ba order along the c -axis in $GdBaCo_2O_x$ arises from the significant difference in ionic radius between Gd^{3+} (1.05 Å) and Ba^{2+} (1.42 Å) [17]. Because this order is thermodynamically stable, achieving a different ion arrangement to modify the functionalities of this type of perovskite requires an unconventional synthesis approach. Previous studies have reported A-site-disordered $Gd_{0.5}Ba_{0.5}CoO_3$ perovskites [18-21]. However, these studies employed high-temperature (above 1000 °C) sintering methods and the obtained lattice parameters closely resembled those of A-site-ordered $GdBaCo_2O_x$, thus suggesting the presence of a Gd/Ba order. In addition, the low-temperature insulating and antiferromagnetic behaviors observed in these studies starkly contrasted the expected characteristics of A-site-disordered $GdBaCo_2O_6$, as discussed later. To the best of our knowledge, the synthesis of both A-site-ordered and -disordered structures in the $RBaCo_2O_6$ family (R = rare-earth element) is limited to $LaBaCo_2O_6$. Since La^{3+} has a larger ionic radius (1.16 Å) than Gd^{3+} , the thermodynamic energy difference between A-site-ordered and -disordered structures is very small for $LaBaCo_2O_6$, and, in fact, the A-site-disordered structure is obtained through conventional high-

temperature processes [22,23].

In this study, we explored synthesis approaches that could achieve cation placement beyond thermodynamically stable sites and investigated the influence of cation position on the magnetic properties of the resultant perovskites. Using a combination of substrate-induced strain and low-temperature topochemical oxidation reactions, we successfully synthesized A-site-disordered $\text{GdBaCo}_2\text{O}_6$ films in which the thermodynamically stable $\text{Gd}^{3+}/\text{Ba}^{2+}$ order was disrupted. Surprisingly, the A-site-disordered $\text{GdBaCo}_2\text{O}_6$ film exhibited metallic and ferromagnetic behaviors, including higher magnetization (11.5 $\mu\text{B}/\text{f.u.}$ at 40 kOe), a higher Curie temperature ($T_C = 165$ K), and lower resistivity (ρ) compared with the A-site-ordered film (9.5 $\mu\text{B}/\text{f.u.}$ at 40 kOe; $T_C = 115$ K). Theoretical calculations predicted that the alterations in the magnetic and conductive properties of the A-site-disordered $\text{GdBaCo}_2\text{O}_6$ film stem from a change in its Co spin states associated with a change in ion arrangement.

2. Experimental

As-grown $\text{GdBaCo}_2\text{O}_x$ films were fabricated using pulsed laser deposition (PLD). $\text{SrTiO}_3(001)$ (STO) and $\text{LaSrGaO}_4(001)$ (LSGO) substrates were used in this study. STO and LSGO have square in-plane lattices with $a = 3.905$ and 3.843 Å, respectively. Bulk $\text{GdBaCo}_2\text{O}_{5.5}$ has an orthorhombic structure with lattice parameters of $a = 3.879$, $b/2 = 3.910$, and $c/2 = 3.768$ Å; therefore, the lattice parameters of the materials show the order $b/2$ (bulk) $>$ a (STO) $>$ a (bulk) $>$ a (LSGO) $>$ $c/2$ (bulk). During the deposition, the substrate temperature and oxygen partial pressure were set to 900 °C and 200 mTorr, respectively, as described in our previous report [7]. A KrF excimer laser (wavelength = 248 nm) with an energy of 1 J cm^{-2} shot^{-1} and repetition rate of 2 Hz was used to ablate $\text{GdBaCo}_2\text{O}_{6-\delta}$ ceramic pellet. The as-grown films were reacted with an aqueous NaClO solution at 80 °C for 40 h to obtain the $x = 6$ phase. At present, stoichiometric A-site-ordered $R\text{BaCo}_2\text{O}_6$ ($R = \text{Pr}$, Gd , and Y) is prepared via low-temperature topotactic oxidation using NaClO solution [6,24–27]. The film thickness

obtained is typically 30–40 nm. The crystal structures of the films were evaluated using X-ray diffraction (XRD) measurements. Their magnetic properties were analyzed using a superconducting quantum interference device magnetometer (MPMS XL, Quantum Design Co.). Magnetization versus temperature measurements were conducted at magnetic field of 500 Oe. The thickness of the films was determined through X-ray reflectivity measurements, while the area of the films was evaluated from photographs taken from the out-of-plane direction of the film. The resistivities of the films were measured using the four-probe method with Au electrodes.

Theoretical density functional theory (DFT)-based calculations were performed using the Vienna ab initio simulation package [28] to investigate the electronic structures of the films. The generalized gradient approximation method developed by Perdew et al. [29] was employed for the exchange-correlation functional. The localized nature of d (f) electrons in Co (Gd) was treated using the GGA + U method with a U value of 5.0 eV [30]. Valence states were described using the plane-wave basis method with a cutoff energy of 800 eV, while core electrons were considered using the projector-augmented wave method [31,32]. Brillouin zone integration was carried out in the Monkhorst–Pack scheme [33] with a Γ -centered $9 \times 9 \times 6$ k-point mesh. The calculations were performed for a doubled unit cell. The experimental lattice constants were used and the atomic positions were relaxed such that the residual force on the atoms was less than 0.01 eV/Å.

3. Results and discussion

3.1. Synthesis of disordered and ordered phases

Figure 1(a, b) shows the out-of-plane XRD 2θ - θ patterns for the as-grown GdBaCo₂O _{x} films on the STO and LSGO substrates. Both films show superlattice (SL) peaks at $2\theta = 11$ – 12° . For bulk GdBaCo₂O_{5.5}, two types of superlattice (SL) peaks appear at $2\theta = 11$ – 12° , which could be indexed to the SL 010 and SL 001 peaks [5]. The SL 010 peak originates from the CoO₆/CoO₅ order along the b -

axis, whereas the SL 001 peak originates from the Gd/Ba order along the c -axis. Therefore, the diffraction peak at $2\theta = 11\text{--}12^\circ$ for the as-grown films indicates the existence of the $\text{CoO}_6/\text{CoO}_5$ or Gd/Ba order in the out-of-plane direction. The calculated out-of-plane lattice constants of the films on the STO and LSGO substrates are 7.529 and 7.837 Å, respectively, which closely match the c - and b -axis lengths of bulk $\text{GdBaCo}_2\text{O}_{5.5}$ (7.535 and 7.820 Å, respectively) [5]. This result suggests that the films on the STO and LSGO substrates are oriented along the c - and b -axis, respectively. Reciprocal space mapping (RSM) measurements confirmed the coherent growth of the films on the substrates, with in-plane lattice constants of 3.905 Å on the STO substrate and 3.843 Å on the LSGO substrate (Fig. S1). Unlike the out-of-plane XRD patterns, the in-plane XRD 2θ - θ patterns showed no SL peaks (Fig. S2), indicating the absence of a long-range ionic order in the in-plane direction. This lack of ionic ordering is attributed to the substrate-induced orthorhombic-to-tetragonal transformation of $\text{GdBaCo}_2\text{O}_x$. However, we utilized our laboratory's XRD equipment without employing techniques such as synchrotron radiation. Therefore, while the degree of ordering is low, there is a possibility that the films still have some short-range ionic ordering (Fig. S2).

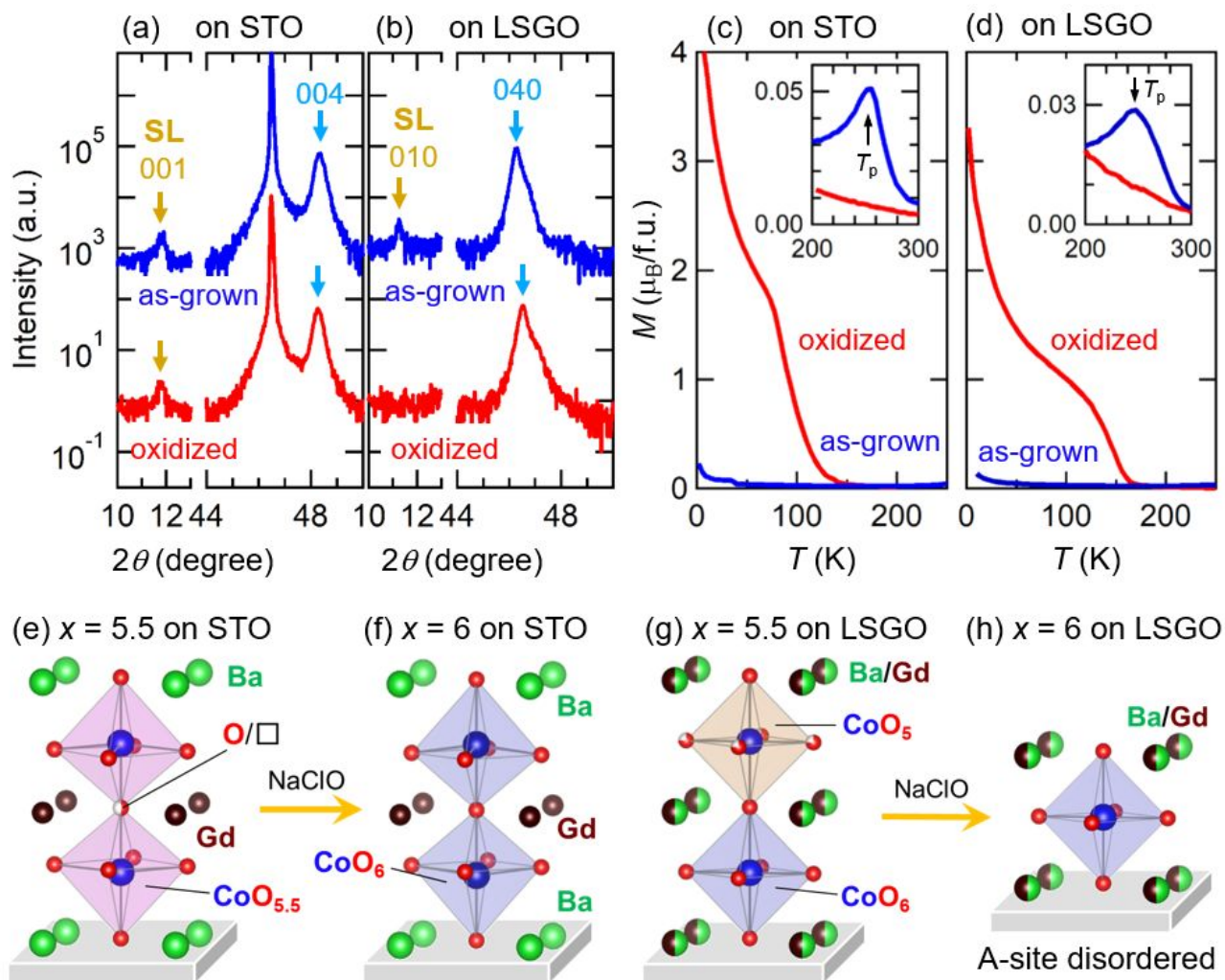


Figure 1. Out-of-plane 2θ - θ XRD patterns for the as-grown and oxidized films on (a) STO and (b) LSGO. (c, d) In-plane magnetization (M)-temperature (T) curves for the samples. The insets show the magnified images. Schematic crystal structures of (e, g) $x = 5.5$ (as-grown) and (f, h) $x = 6$ (oxidized) films on the (e, f) STO and (g, h) LSGO substrates.

The magnetic properties of perovskite cobaltates are strongly influenced by the oxidation state of Co. Figure 1(c, d) shows the in-plane magnetization (M)-temperature (T) curves for the as-grown films on STO and LSGO. The M - T curves for both films exhibit positive peaks at approximately 250 K (T_p in the figures), similar to the behavior observed in bulk $\text{GdBaCo}_2\text{O}_x$ with $x = 5.33$ - 5.55 [5], which is attributed to the ferromagnetic-to-antiferromagnetic phase transition. This result suggests that

the as-grown films have an approximate x value of 5.5. Subsequently, the as-grown films were oxidized by treatment with NaClO solution at 80 °C for 40 h, following the same procedure reported for the fabrication of A-site-ordered GdBaCo₂O₆ films [6]. In contrast to the as-grown films, the oxidized films exhibit ferromagnetic behavior below T_C . Moreover, the M values of the oxidized films are significantly higher than those of the as-grown films, which confirms successful oxidation via NaClO treatment. The oxidation state of Co ions was also evaluated using X-ray absorption spectroscopy measurements (Fig. S4), showing that the Co ions exist as Co³⁺ in the as-grown film and a mixture of Co³⁺ and Co⁴⁺ in the oxidized films. Hereafter, the as-grown and oxidized films are referred to as $x = 5.5$ and 6 films, respectively. It is noted that there is no direct evidence proving the oxygen content is exactly six in the oxidized film. This issue arises from the nature of oxide thin films, and obtaining such evidence is extremely difficult as long as oxide thin films are used. There are two main reasons why accurately quantifying the oxygen content in oxide thin films is difficult: first, the film has a very small volume, and second, the substrate also contains oxygen.

Figure 1(a, b) also depicts the out-of-plane XRD patterns of the $x = 6$ films. The $x = 6$ film on the STO substrate retains its SL 001 peak at $2\theta = 11^\circ$, indicating the maintenance of the Gd/Ba order during oxidation. It is noted that in the case of GdBaCo₂O_{5.5}, the presence of superlattice peaks suggests the possibility of two types of ordering: Gd/Ba or oxygen defects. However, in the case of GdBaCo₂O₆, oxygen vacancies do not order, and the superlattice peaks solely originate from Gd/Ba ordering. By contrast, the SL peak at $2\theta = 11^\circ$ disappeared for the $x = 6$ film on the LSGO substrate, indicating the disappearance of the CoO₆/CoO₅ order during oxidation. This finding is reasonable because CoO₅ is transformed into CoO₆ during oxidation. The out-of-plane lattice constants of the $x = 6$ films on the STO and LSGO substrates are 7.538 ($= 2 \times 3.769$) and 3.900 Å, respectively. Conversely, the in-plane lattice constants measured using RSM (Fig. S3) are consistent with those of the as-grown films and substrates (3.905 and 3.843 Å, respectively). However, in the RSM pattern, a q_x tail was also observed, indicating that partial relaxation appears in the film on LSGO during the oxidation process. Compared to the RSM

results of the films on STO and LSGO substrates, the full width at half maximum (FWHM) values of the curves in the q_x direction for the 103 diffraction peak was different (Figs. S1 and S3). The FWHM values for the as-grown films on STO and LSGO substrates were 0.002 and 0.007 nm⁻¹, respectively, while those for the oxidized films on these substrates were 0.003 and 0.016 nm⁻¹, respectively. This result suggests that the crystallinity of the films on LSGO substrates is worse than that of the films on STO substrates.

We also performed structural optimization of A-site ordered GdBaCo₂O_{5.5} and GdBaCo₂O₆ thin films using DFT calculations. Figure S5 shows the relationship between the c -axis length and energy of GdBaCo₂O_{5.5} and GdBaCo₂O₆. Here, the a - and b -axis lengths were fixed at 3.905 Å. Comparing the c -axis lengths at the energy minima, it was observed that the c -axis length of GdBaCo₂O₆ is slightly longer than that of GdBaCo₂O_{5.5}, consistent with the trends observed in the films on STO substrates. This behavior is not typically observed in perovskite oxides, where the volume tends to decrease when oxygen vacancies are reduced. Indeed, the volume of the A-site disordered films on LSGO substrates decreases with increasing the oxygen content. As for the bulk A-site ordered GdBaCo₂O _{x} , c -axis length increases but cell volume decreases with increasing x when $5.5 < x < 5.77$ [5]. Hence, the presence of Gd/Ba ordering and the epitaxial strain from the substrate is crucial for modifying the cell volume during oxidation.

Table S1 shows the intensity ratio of the 001 to 006 peak (I_{001}/I_{006}) for the as-grown and oxidized films on STO substrates, together with the simulation results (see Reply2-4). In both the experiment and simulation, the I_{001}/I_{006} value increases with oxidation. However, there is a difference between the experimental and simulation results; the I_{001}/I_{006} values for the $x = 5.5$ and 6 films were 84% and 59% of the theoretical values, respectively. Based on the obtained values, the ordering ratio is estimated to be 92% and 77% for the as-grown and $x = 6$ films, respectively. However, the ordering ratio may differ from the actual value because the DFT calculation assumes 0 K, whereas the XRD measurements were conducted at room temperature.

Figure 1(e–h) shows schematic images illustrating the synthesis process and crystal structures

of the films. The $x = 5.5$ films on the STO and LSGO substrates exhibit Gd/Ba and $\text{CoO}_6/\text{CoO}_5$ orders, respectively, along the out-of-plane direction. However, no long-range ionic orders are observed along the in-plane direction owing to the strain induced by the substrates. After their reaction with NaClO, the films undergo oxygen-ion insertion. The $x = 6$ film on STO maintains its Gd/Ba order along the out-of-plane direction. By contrast, the $x = 6$ film on the LSGO substrate lacks long-range orders, indicating an A-site-disordered structure.

3.2. Magnetic properties

Figure 2(a, b) shows the $M-H$ curves for the A-site-ordered and -disordered $x = 6$ films as a function of the H direction. Both films display distinct magnetic hysteresis loops, thus confirming their ferromagnetic nature. The M value at $H = 40$ kOe of the A-site-ordered $x = 6$ film is $9.5 \mu_{\text{B}}/\text{f.u.}$, which is $2 \mu_{\text{B}}/\text{f.u.}$ smaller than that of the A-site-disordered $x = 6$ film ($11.5 \mu_{\text{B}}/\text{f.u.}$). This result suggests a difference in Co spin states between the A-site-ordered and -disordered $x = 6$ films. These films show magnetic anisotropy. As for the A-site-ordered $x = 6$ film, the remnant magnetization (M_r) and coercive magnetic field (H_c) in the in-plane direction, $4.8 \mu_{\text{B}}/\text{f.u.}$ and 0.5 kOe, respectively, are much larger than those in the out-of-plane direction, $0.5 \mu_{\text{B}}/\text{f.u.}$ and 0.2 kOe, showing the strong magnetic anisotropy along the in-plane direction. On the other hand, M_r of the A-site-disordered $x = 6$ film in the in-plane direction ($4.9 \mu_{\text{B}}/\text{f.u.}$) is smaller than that in the out-of-plane direction ($3.0 \mu_{\text{B}}/\text{f.u.}$), indicating the perpendicular magnetic anisotropy. This indicates that the magnetic anisotropy properties of the A-site-disordered film are not determined by the film's shape because the thin film geometry typically result in in-plane magnetic anisotropy. However, in the A-site disordered film, the H_c value in the in-plane direction is similar to that in the perpendicular direction, suggesting that the magnetic anisotropy is small. The magnetic anisotropy constant (K_u) was evaluated from the area enclosed between the in-plane and out-of-plane $M-H$ curves below 50 kOe (Fig. S4). The K_u value of the A-site-ordered $x = 6$ film ($-1.7 \times 10^7 \text{ erg/cm}^3$) is five times larger than that of the A-site-disordered $x = 6$ film (3×10^6

erg/cm³). Notably, the magnetization of the A-site ordered film doesn't reach its saturation point even when subjected to a magnetic field of 50 kOe. This is probably because of the differing magnetic anisotropic properties between the Gd and Co magnetic moments. We estimate that 50 kOe isn't sufficient to fully align the Co ions' magnetic moment in the out-of-plane direction. This finding highlights the effectiveness of the A-site-ordering system in enhancing magnetic anisotropy.

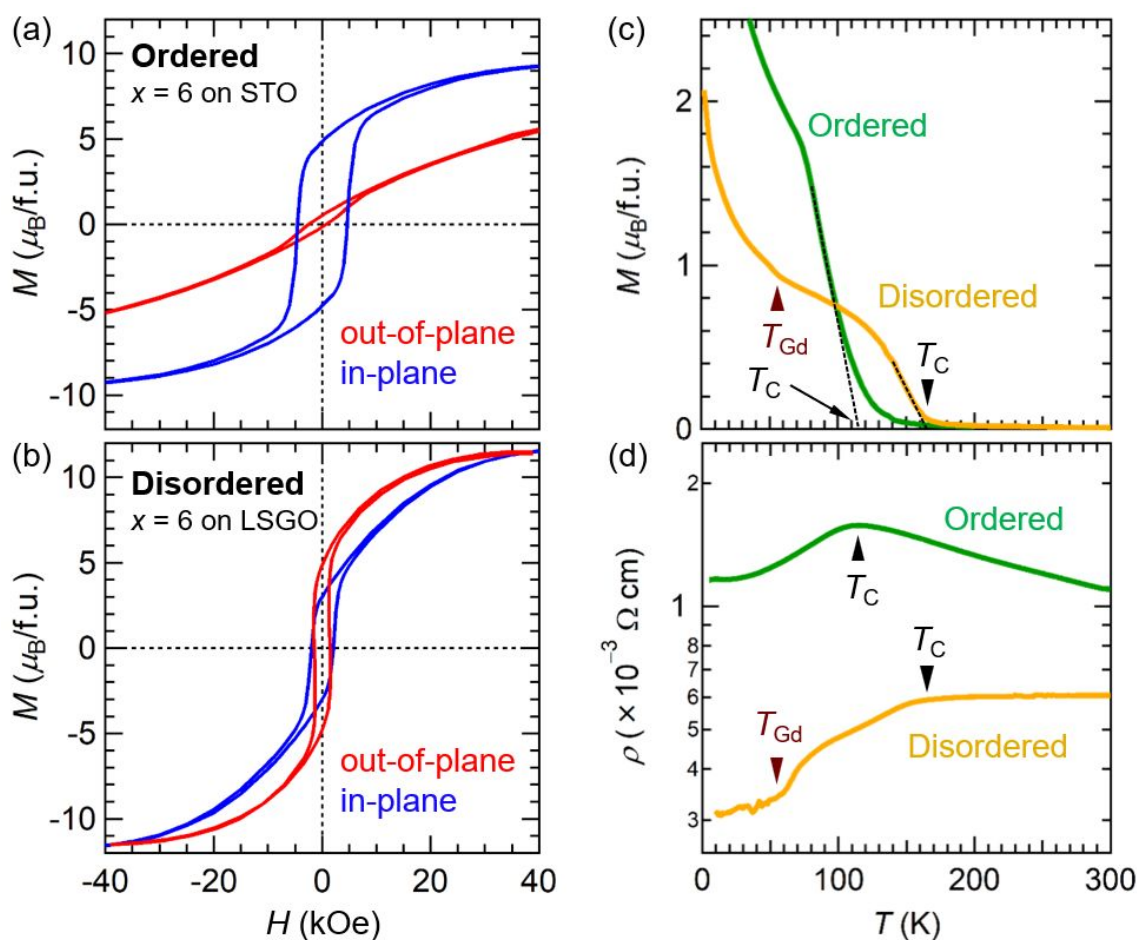


Figure 2. In-plane and out-of-plane magnetization (M)–magnetic field (H) curves for the (a) A-site-ordered $x = 6$ film at 2 K and (b) A-site-disordered $x = 6$ film at 5 K. (c) M –temperature (T) and (d) resistivity (ρ)– T curves for the A-site-ordered and -disordered $x = 6$ films. In Figure (c), a magnetic field of 500 Oe is applied along the direction of the easy magnetization axis: in-plane and out-of-plane direction in the A-site-ordered and -disordered $x = 6$ films, respectively.

Figure 2(c) shows the M - T curves for the A-site-ordered and -disordered $x = 6$ films. The T_C of the A-site-ordered $x = 6$ film is 115 K, which is lower than that of the A-site-disordered $x = 6$ film (165 K), indicating the importance of cation disordering in T_C . In the disordered $x = 6$ film, the M values exhibit an abrupt increase below 60 K, which is denoted as T_{Gd} in the figure. This behavior arises from the difference in the temperature dependence of the sublattice magnetization at the $Gd^{3+} 4f^7$ and $Co^{3.5+} 3d^{5.5}$ sites; the sublattice magnetization at the Gd sites decreases above T_{Gd} , while that at the Co sites decreases above T_C .

Figure 2(d) shows the ρ - T curves for the A-site-ordered and -disordered $x = 6$ films. The A-site-ordered $x = 6$ film displays metallic behavior ($d\rho/dT > 0$) below T_C and semiconducting behavior ($d\rho/dT < 0$) above T_C . By contrast, the A-site-disordered $x = 6$ film exhibits only metallic behavior below 300 K. The ρ values of the A-site-disordered $x = 6$ film are lower than those of the A-site-ordered $x = 6$ film. Notably, in the ρ - T curve of the A-site-disordered $x = 6$ film, two kinks appear near the magnetic phase transition (T_{Gd} and T_C). Some cobaltites exhibit charge ordering. For instance, in $YBaCo_2O_5$, Co^{2+} and Co^{3+} are indeed ordered [34]. However, such charge ordering typically occurs in the insulating state. On the other hand, $GdBaCo_2O_6$ exhibits a metallic state, indicating that electrons at the Fermi energy can move freely between adjacent Co orbitals. Therefore, we do not expect charge ordering in the film.

3.3. Effect of ion arrangement on magnetism

Table 1 shows a comparison of the lattice constants and magnetic and conductive properties of the A-site-ordered and -disordered $x = 6$ films. The A-site-ordered $x = 6$ film on the STO substrate has a tetragonal structure, in which the out-of-plane lattice constant is 3.5% smaller than the in-plane lattice constant. By contrast, the out-of-plane lattice constant of the A-site-disordered $x = 6$ film on the LSGO substrate is 1.4% larger than the in-plane lattice constant. In terms of magnetism, the A-site-disordered

$x = 6$ film demonstrates a higher T_C and larger M at 40 kOe than the A-site-ordered $x = 6$ film. Moreover, the A-site-disordered $x = 6$ film exhibits lower ρ and maintains its metallic behavior even above T_C .

Table 1. Structural, magnetic, and electric properties of the A-site-ordered and -disordered $x = 6$ films.

	A-site-ordered $x = 6$ film on STO	A-site-disordered $x = 6$ film on LSGO
Out-of-plane and in-plane lattice constant (\AA)	7.538 ($= 2 \times 3.769$) and 3.905	3.900 and 3.843
T_C (K)	115	165
M at 40 kOe ($\mu_B/\text{f.u.}$)	9.5	11.5
K_u (erg/cm ³)	-1.7×10^7	3×10^6
$d\rho/dT$	>0 (below T_C) and <0 (above T_C)	>0
Schematic representation of the DOS of Co orbitals		
PDOS of Co at E_F	$3d e_g$ (spin-up)	$3d e_g$ (spin-up) and $3d t_{2g}$ (spin-down)

DFT calculations were performed to elucidate the origins of the difference in magnetism between the films. A-site-ordered $\text{GdBaCo}_2\text{O}_6$ has a structure in which the GdO and BaO layers are stacked along the c -axis (Fig. 3(a)), and this arrangement is uniquely determined. However, for the A-site-disordered $x = 6$ film, experimental ion ordering was not observed. In such cases, the most appropriate approach is to prepare an extensive cell size, randomly place Gd and Ba ions, and perform calculations. However, DFT calculations require a significant amount of time because of the substantial number of atoms. Therefore, we performed DFT calculations for the three different Gd/Ba configurations depicted in Fig. 3(b–d) by setting the same lattice constants as those for the A-site-disordered $x = 6$ film. Hereafter, the structures shown in Fig. 3(b–d) are referred to as 0D-, 1D-, and 2D-GBCO, respectively. Among these structures, the total energy of 2D-GBCO is the lowest; thus, this structure is the most stable. This finding may probably be attributed to the shift of Co ions away from the center of CoO_6 . In this study, we obtained a $\text{GdBaCo}_2\text{O}_6$ film not through direct growth but

by the low-temperature oxidation of a $\text{GdBaCo}_2\text{O}_{5.5}$ film with the $\text{CoO}_6/\text{CoO}_5$ order. We speculate that the presence of the $\text{CoO}_6/\text{CoO}_5$ order in $\text{GdBaCo}_2\text{O}_{5.5}$ also causes a Co-ion shift, which stabilizes the structure even when the cation arrangement does not match that of 2D-GBCO. However, our DFT calculations indicate that as the oxygen content reaches $x = 6$, the off-center displacement of Co-ions decreases with decreasing of A-site ordering degree.

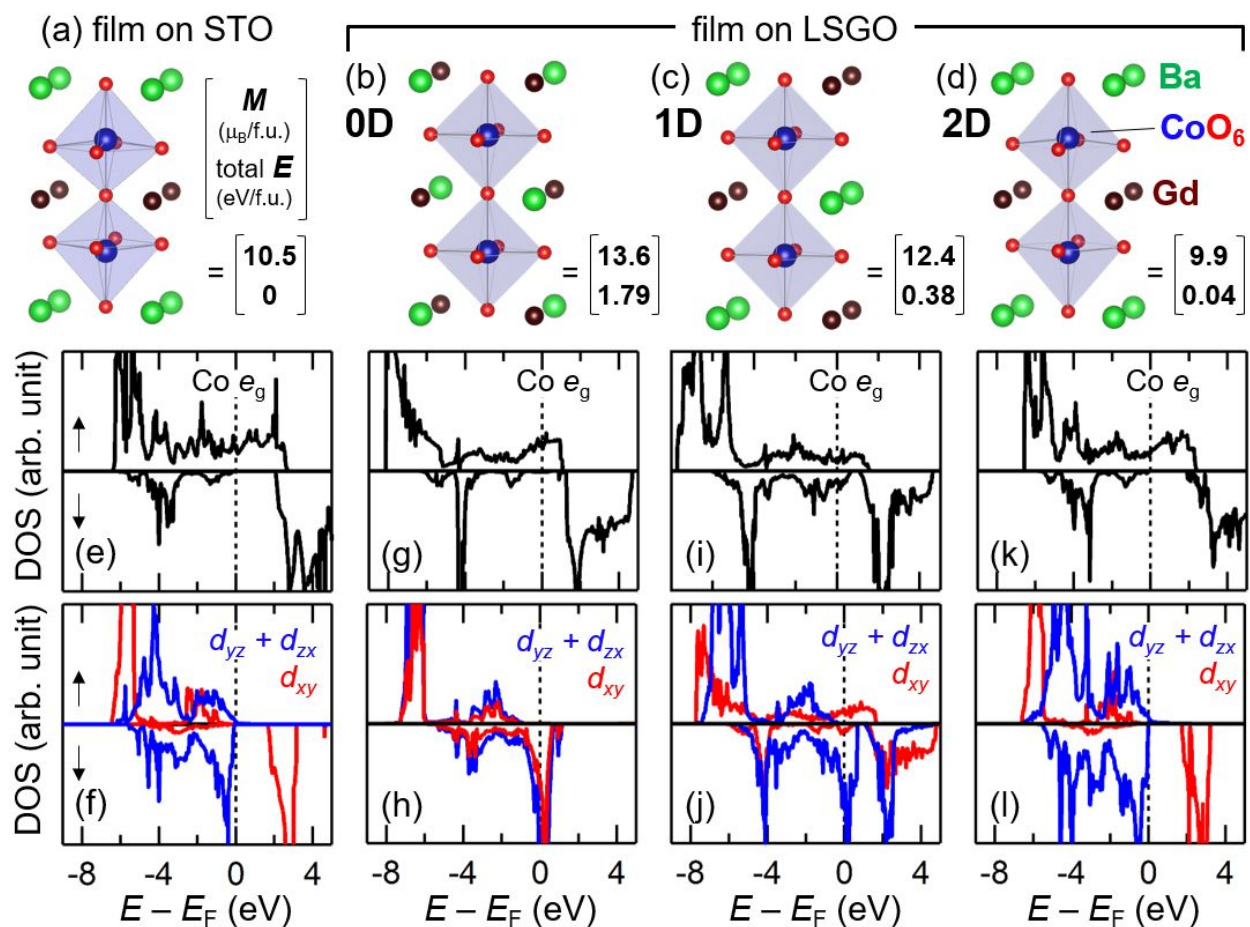


Figure 3. Crystal structures and partial densities of states (DOS) of Co orbitals for (a, e, f) $\text{GdBaCo}_2\text{O}_6$ films on STO and (b, g, h) 0D-, (c, i, j) 1D-, and (d, k, l) 2D-GBCO films on LSGO.

Figure 3(e, f) shows the partial densities of states (DOS) of the Co orbitals calculated for the A-site-ordered $x = 6$ film grown on the STO substrate. In accordance with the difference in the spin-

up and spin-down DOS spectra, the total magnetization was calculated to be $10.5 \mu_B/\text{f.u.}$, which closely agreed with the experimental results ($M = 9.5 \mu_B/\text{f.u.}$ at 40 kOe, Fig. 2(a)). Notably, only the spin-up Co $3d e_g$ and O $2p$ orbitals exhibit a finite DOS at the Fermi energy (E_F), indicating the half-metallicity of the film. The total magnetization consists of two types of sublattice magnetizations: Gd $4f^7$ and Co $3d^{5.5}$. Considering that the sublattice magnetization of Gd $4f^7$ is $7 \mu_B/\text{f.u.}$, the Co orbital represents a mixed state of intermediate-spin Co^{3+} and low-spin Co^{4+} , resulting in half-metallicity through a double-exchange interaction.

Figure 3(g–l) shows the partial DOS of the Co orbitals as a function of the ion arrangement. The calculations were performed using the same lattice constants as those of the experimental film on the LSGO substrate. The total magnetization values for 0D-, 1D-, and 2D-GBCO are 13.6, 12.4, and $9.9 \mu_B/\text{f.u.}$, respectively, indicating the significant influence of ion arrangement on the Co spin states. For example, in 2D-GBCO, similar to the film on the STO substrate (Fig. 3(e, f)), the spin-down d_{xy} orbital is unoccupied, whereas the spin-down d_{yz} and d_{zx} orbitals are occupied by electrons, resulting in a hybrid state of intermediate-spin Co^{3+} and low-spin Co^{4+} , which contributes to the half-metallic character of the film. Conversely, in 0D-GBCO, in which the d_{xy} , d_{yz} , and d_{zx} orbitals possess the same energy, the DOS for the spin-down $3d t_{2g}$ orbitals appears at E_F . Therefore, the Co ions in 0D-GBCO adopt a mixed state of high-spin Co^{3+} and intermediate-spin Co^{4+} . In general, Co spin state strongly depends on the energy of the Co $3d$ orbitals. When CoO_6 has high symmetry, where the lattice constants are $a = b = c$ and the Co position is at the center of CoO_6 , the Co $3d$ orbitals in CoO_6 split into t_{2g} ($3d_{xy}$, $3d_{yz}$, $3d_{zx}$) and e_g ($3d_{x^2-y^2}$, $3d_{z^2}$) states. On the other hand, when the lattice constants change to $a = b \neq c$ with keeping the Co position at the center of CoO_6 , further splitting occurs into $3d_{xy}$, ($3d_{yz}$, $3d_{zx}$), $3d_{x^2-y^2}$, and $3d_{z^2}$ states. Moreover, when the Co position shifts from the center of CoO_6 , this splitting widens further. In this study, DFT calculations revealed that the arrangement of Gd/Ba orders leads to variations in the Co position within CoO_6 ; unlike 0D-GBCO, 2D-GBCO features Co ions that shift away from the center of CoO_6 . This change in symmetry alters the energy of the Co $3d$ orbitals, consequently affecting the spin state.

Table 1 provides schematic representations of the partial DOS for Co orbitals in A-site-ordered and -disordered $x = 6$ films grown on the STO and LSGO substrates, respectively. The Co $3d t_{2g}$ states of the films differ because of variations in their ion arrangement. In the A-site-disordered film, the appearance of spin-down t_{2g} orbitals at E_F enhances its electrical conductivity (Fig. 2(d)). Additionally, the reduction in the DOS of the spin-down t_{2g} orbitals below E_F contributes to an increase in the magnetic moment of the Co ions, leading to enhancements in magnetization and T_C compared with the A-site-ordered film (Fig. 2).

The relationship between ion arrangement and magnetic properties for several double-perovskite $AA'BB'O_6$ systems has been reported [1-3,17,35-38]. For example, B-site-ordered Sr_2FeMoO_6 shows room-temperature ferrimagnetism owing to the magnetic coupling between Fe and Mo ions [1]. The ion arrangement in A-site-ordered and -disordered $RBaMn_2O_6$ influences the distance between neighboring Mn ions as well as the anisotropic properties of Mn orbitals, resulting in the modulation of magnetic properties [2]. In A-site-ordered $RBaMn_2O_6$ ($R = La, Pr$ and Nd), ferromagnetic double exchange interaction is dominant, while the ground state is a mixture of ferromagnetic and antiferromagnetic charge-orbital ordered phases for $R = La$ and A-type antiferromagnetic phase for $R = Pr$ and Nd [39]. These ground state behaviors are explained by the effect of Mn–O distance on the bandwidth and the two-dimensional character in the structure [39]. In $GdBaCo_2O_6$, the ion arrangement affects the spin states of Co ions, leading to the modulation of its magnetic and electric conduction properties.

Finally, we discuss the difference in K_u between the A-site-ordered and -disordered $x = 6$ films. In general, the direction of magnetic anisotropy in cobaltates is determined by the coordination environment. In the A-site-ordered $x = 6$ film, the out-of-plane length of CoO_6 octahedra (l_{oop}) is much shorter than the in-plane length one (l_{ip}); $(l_{oop} - l_{ip})/l_{ip} = -3.5\%$. By contrast, l_{oop} is longer than l_{ip} in the A-site-disordered $x = 6$ film ($(l_{oop} - l_{ip})/l_{ip} = 1.5\%$). This change in the sign of $(l_{oop} - l_{ip})/l_{ip}$ is the origin of the difference in the direction of magnetic anisotropy between the films; the A-site-ordered

$x = 6$ film shows in-plane magnetic anisotropy, whereas the A-site-disordered film shows perpendicular magnetic anisotropy. Additionally, the large value of $(l_{\text{oop}} - l_{\text{ip}})/l_{\text{ip}}$ for the A-site-ordered $x = 6$ film probably leads to the large K_{u} value.

4. Conclusion

In this study, we investigated the effects of cation arrangement on the magnetic properties of $\text{GdBaCo}_2\text{O}_6$. Despite the thermodynamic stability of the Gd/Ba order, our synthesis method, which included substrate-induced strain and low-temperature topochemical reactions, successfully produced A-site-disordered $\text{GdBaCo}_2\text{O}_6$ films. These films displayed notable enhancements in magnetic and electrical properties, including higher M at 40 kOe and T_{C} , perpendicular magnetic anisotropy, and reduced ρ , compared with their A-site-ordered counterparts. Theoretical investigations confirmed that changes in the Co spin states induced these property modifications. Our results highlight the potential of unconventional synthesis strategies for expanding the tunability of functionalities in double-perovskite materials and modulating spin states through cation-placement control.

Acknowledgments

This study was supported by JST PRESTO (JPMJPR21Q3) and JSPS KAKENHI (20H02614). SS thanks Ryotaro Arita for his helpful comments.

Supporting information

See supporting information for the details of XRD of the films.

References

- [1] K. I. Kobayashi, T. Kimura, H. Sawada, K. Terakura, Y. Tokura, Room-temperature magnetoresistance in an oxide material with an ordered double-perovskite structure. *Nature* **395**,

677–680 (1998).

- [2] S. Yamada, N. Abe, H. Sagayama, K. Ogawa, T. Yamagami, T. Arima, Room-temperature low-field colossal magnetoresistance in double-perovskite manganite. *Phys. Rev. Lett.* **123**, 126602 (2019).
- [3] S. Chakraverty, K. Yoshimatsu, Y. Kozuka, H. Kumigashira, M. Oshima, T. Makino, A. Ohtomo, M. Kawasaki, Magnetic and electronic properties of ordered double-perovskite La_2VMnO_6 thin films. *Phys. Rev. B* **84**, 132411 (2011).
- [4] A. A. Taskin, A. N. Lavrov and Y. Ando, Ising-like spin anisotropy and competing antiferromagnetic-ferromagnetic orders in $\text{GdBaCo}_2\text{O}_{5.5}$ single crystals. *Phys. Rev. Lett.* **90**, 227201 (2003).
- [5] A. A. Taskin, A. N. Lavrov, and Y. Ando, Transport and magnetic properties of $\text{GdBaCo}_2\text{O}_{5+x}$ single crystals: A cobalt oxide with square-lattice CoO_2 planes over a wide range of electron and hole doping. *Phys. Rev. B* **71**, 134414 (2005).
- [6] T. Katayama, S. Mo, A. Chikamatsu, Y. Kurauchi, H. Kumigashira, T. Hasegawa, Half-metallicity and magnetic anisotropy in double-perovskite $\text{GdBaCo}_2\text{O}_6$ films prepared via topotactic oxidation. *Chem. Mater.* **35**, 1295 (2023).
- [7] T. Katayama, A. Chikamatsu, Y. Zhang, S. Yasui, H. Wadati, and T. Hasegawa, Ionic-order engineering in double-perovskite cobaltite. *Chem. Mater.* **33**, 5675 (2021).
- [8] M. M. Seikh, C. Simon, V. Caignaert, V. Pralong, M. B. Lepetit, S. Boudin, and B. Raveau, New Magnetic Transitions in the Ordered Oxygen-Deficient Perovskite $\text{LnBaCo}_2\text{O}_{5.50+\delta}$. *Chem. Mater.* **20**, 231-238 (2008).
- [9] C. Martin, A. Maignan, D. Pelloquin, N. Nguyen, and B. Raveau, Magnetoresistance in the oxygen deficient $\text{LnBaCo}_2\text{O}_{5.4}$ ($\text{Ln} = \text{Eu}, \text{Gd}$) phases. *Appl. Phys. Lett.* **71**, 1421 (1997).
- [10] Y. Zhang, T. Katayama, A. Chikamatsu, C. Schubler-Langeheine, N. Pontius, Y. Hirata, K. Takubo, K. Yamagami, K. Ikeda, K. Yamamoto, T. Hasegawa, and H. Wadati, Photo-induced

Antiferromagnetic-ferromagnetic and Spin-state Transition in $\text{GdBaCo}_2\text{O}_{5.5}$ Thin Film. *Commun. Phys.* **5**, 50 (2022).

- [11] A. A. Taskin, A. N. Lavrov, and Y. Ando, Achieving fast oxygen diffusion in perovskites by cation ordering. *Appl. Phys. Lett.* **86**, 091910 (2005).
- [12] A. Tarancón, S. J. Skinner, R. J. Chater, F. Hernández-Ramírez and J. A. Kilner, Layered perovskites as promising cathodes for intermediate temperature solid oxide fuel cells. *J. Mater. Chem.* **17**, 3175–3181 (2007).
- [13] J. Zapata, M. Burriel, P. García, J. A. Kilner and J. Santiso, Anisotropic ^{18}O tracer diffusion in epitaxial films of $\text{GdBaCo}_2\text{O}_{5+\delta}$ cathode material with different orientations. *J. Mater. Chem. A*, **1**, 7408–7414 (2013).
- [14] Y. C. Chen, M. Yashima, J. Peña-Martínez and J. A. Kilner, Experimental visualization of the diffusional pathway of oxide ions in a layered perovskite-type cobaltite $\text{PrBaCo}_2\text{O}_{5+\delta}$. *Chem. Mater.* **25**, 2638–2641 (2013).
- [15] T. Katayama, K. Magara, A. Chikamatsu, and T. Hasegawa, Anisotropic proton conduction in double-perovskite $\text{GdBaCo}_2\text{O}_{5.5}$. *Appl. Phys. Lett.* **XX**, XXXX (2023).
- [16] M. Burriel, M. Casas-Cabanas, J. Zapata, H. Tan, J. Verbeeck, C. Solís, J. Roqueta, S. J. Skinner, J. A. Kilner, G. Tendeloo, and J. Santiso, Influence of the microstructure on the high-temperature transport properties of $\text{GdBaCo}_2\text{O}_{5.5+\delta}$ epitaxial films. *Chem. Mater.* **22**, 5512–5520 (2010).
- [17] A. Ohtomo, S. Chakraverty, H. Mashiko, T. Oshima, and M. Kawasaki, Spontaneous atomic ordering and magnetism in epitaxially stabilized double perovskites. *J. Mater. Res.* **28**, 689, (2013).
- [18] I. O. Troyanchuk, N. V. Kasper, D. D. Khalyavin, H. Szymczak, R. Szymczak, and M. Baran, Phase Transitions in the $\text{Gd}_{0.5}\text{Ba}_{0.5}\text{CoO}_3$ Perovskite. *Phys. Rev. Lett.* **80**, 3380 (1998).
- [19] I. O. Troyanchuk, D. D. Khalyavin, T. K. Solovykh, H. Szymczak, Q. Huang, and J. W. Lynn, Magnetic and crystal structure phase transitions in $R_{1-x}\text{Ba}_x\text{CoO}_{3-y}$ ($R = \text{Nd, Gd}$). *J. Phys.:*

Condens. Matter. **12**, 2485 (2000).

- [20] P. V. Vanitha, A. Arulraj, P. N. Santhosh, and C. N. R. Rao, Effect of cation size and disorder on the structure and properties of the rare earth cobaltates, $\text{Ln}_{0.5}\text{A}_{0.5}\text{CoO}_3$ (Ln = Rare Earth, A = Sr, Ba). *Chem. Mater.* **12**, 1666 (2000).
- [21] A. K. Kundu, and C. N. R. Rao, Cation size disorder as the crucial determinant of the unusual magnetic and electronic properties of $\text{Gd}_{0.5}\text{Ba}_{0.5}\text{CoO}_3$. *J. Phys.: Condens. Matter.* **16**, 415–425 (2004).
- [22] T. Nakajima, M. Ichihara, and Y. Ueda, New A-site ordered perovskite cobaltite $\text{LaBaCo}_2\text{O}_6$: synthesis, structure, physical property and cation order–disorder effect. *J. Phys. Soc. Jpn.* **74**, 1572–1577 (2005).
- [23] E. Rautama, P. Boullay, A. K. Kundu, V. Caignaert, V. Pralong, M. Karppinen, and B. Raveau, Cationic ordering and microstructural effects in the ferromagnetic perovskite $\text{La}_{0.5}\text{Ba}_{0.5}\text{CoO}_3$: impact upon magnetotransport properties. *Chem. Mater.* **20**, 2742–2750 (2008).
- [24] M. M. Seikh, V. Pralong, O. I. Lebedev, V. Caignaert, and B. Raveau, The ordered double perovskite $\text{PrBaCo}_2\text{O}_6$: synthesis, structure, and magnetism. *J. Appl. Phys.* **114**, 013902 (2013).
- [25] M. Goto, T. Saito, and Y. Shimakawa, Unusual ferromagnetic metal: A-site-layer-ordered double perovskite YBaCo_2O_6 with unusually high valence $\text{Co}^{3.5+}$. *Chem. Mater.* **30**, 8702–8706 (2018).
- [26] T. Katayama, A. Chikamatsu, Y. Hirose, M. Minohara, H. Kumigashira, I. Harayama, D. Sekiba, and T. Hasegawa, Ferromagnetism with strong magnetocrystalline anisotropy in A-site ordered perovskite YBaCo_2O_6 epitaxial thin films prepared via wet-chemical topotactic oxidation. *J. Mater. Chem. C* **6**, 3445–3450 (2018).
- [27] A. Chikamatsu, T. Katayama, T. Maruyama, M. Kitamura, K. Horiba, H. Kumigashira, H. Wadati, and T. Hasegawa, Investigation of the electronic states of A-site layer-ordered double perovskite YBaCo_2O_x ($x = 5.3$ and 6) thin films by X-ray spectroscopy. *Appl. Phys. Lett.* **118**,

012401 (2021).

- [28] Kresse, G.; Furthmüller, J. Efficient Iterative Schemes for ab initio Total-energy Calculations using A Plane-wave Basis Set. *Phys. Rev. B* **54**, 11169–11186 (1996).
- [29] Perdew, J. P.; Burke, K.; Ernzerhof, M. Generalized Gradient Approximation Made Simple. *Phys. Rev. Lett.* **77**, 3865–3868 (1996).
- [30] Coulaud, E.; Dezanneau, G.; Geneste, G. Hydration, oxidation, and reduction of $\text{GdBaCo}_2\text{O}_{5.5}$ from first-principles. *J. Mater. Chem. A* **3**, 23917 (2015).
- [31] Blöchl, P. E. Projector Augmented-wave Method. *Phys. Rev. B* **50**, 17953–17979 (1994).
- [32] Kresse, G.; Joubert, D. From Ultrasoft Pseudopotentials to the Projector Augmented-wave Method. *Phys. Rev. B* **59**, 1758–1775 (1999).
- [33] Monkhorst, H.; Pack, J. D. Special Points for Brillouin-zone Integrations. *Phys. Rev. B* **13**, 5188–5192 (1976).
- [34] Vogt, T.; Woodward, P. M.; Karen, P.; Hunter, B. A.; Henning, P.; Moodenbaugh, A. R. Low to High Spin-State Transition Induced by Charge Ordering in Antiferromagnetic YBaCo_2O_5 . *Phys. Rev. Lett.* **2000**, *84*, 2969–2972.
- [35] Vasala, S.; Karppinen, M. $\text{A}_2\text{B}'\text{B}''\text{O}_6$ perovskites: A review. *Prog. Solid State Chem.* **43** 1–36 (2015).
- [36] L. Jin, D. Ni, X. Gui, D. B. Straus, Q. Zhang, and R. J. Cava, Ferromagnetic Double Perovskite Semiconductors with Tunable Properties. *Adv. Sci.* **9**, 2104319 (2022).
- [37] R. C. Sahoo, Y. Takeuchi, A. Ohtomo, and Z. Hossain, Exchange bias and spin glass states driven by antisite disorder in the double perovskite compound LaSrCoFeO_6 . *Phys. Rev. B* **100**, 214436 (2019).
- [38] K. Yoshimatsu, J. Ishimaru, K. Watarai, K. Yamamoto, Y. Hirata, H. Wadati, Y. Takeda, K. Horiba, H. Kumigashira, O. Sakata, and A. Ohtomo, Magnetic and electronic properties of B-site-ordered double-perovskite oxide $\text{La}_2\text{CrMnO}_6$ thin films. *Phys. Rev. B* **99**, 235129 (2019).

T. Nakajima, H. Kageyama, H. Yoshizawa, K. Ohoyama, and Y. Ueda, Ground State Properties of the A-site Ordered Manganites, $RBaMn_2O_6$ ($R = \text{La, Pr and Nd}$). *J. Phys. Soc. Japan* **72**, 3237 (2003).

The data supporting this article have been included as part of the Supplementary Information.